Dynamics of a silicone oil drop submerged in a stratified ethanol-water bath

Miguel A. Herrada,[1] José M. Montanero,[2] and Luis Carrión[3]
[1]*E.S.I., Universidad de Sevilla, Camino de los Descubrimientos s/n 41092, Spain*
[2]*Depto. de Ingeniería Mecánica, Energética y de los Materiales and Instituto de Computación Científica Avanzada (ICCAEx), Universidad de Extremadura, E-06006 Badajoz, Spain*
[3]*DCEM, Universidad de las Fuerzas Armadas-ESPE, Ave. Gral. Rumiñahui s/n, Sangolquí, Pichincha 171103, Ecuador*

(Received 19 July 2023; accepted 17 November 2023; published 7 December 2023)

We analyze numerically the Marangoni flow around an immiscible droplet submerged in a stably stratified mixture of ethanol and water. The linear stability analysis shows that the base flow undergoes a supercritical Hopf bifurcation that leads to oscillations. The theoretical prediction for the critical droplet radius is consistent with previous experimental results. Ethanol diffusion in water is critical in the flow stability for both low and high droplet viscosity. Direct numerical simulations of the nonlinear oscillatory flow show that the frequency of those oscillations approximately equals that of the critical eigenmode. The nonlinear convective term of the ethanol diffusive-convective transport equation fixes the amplitude of the droplet oscillations. The viscous dissipation associated with the Marangoni flow inside the droplet considerably reduces the oscillation.

DOI: 10.1103/PhysRevE.108.065104

I. INTRODUCTION

A concentration or temperature gradient applied to an interface can induce Marangoni steady convection. This convection can suffer from instability, which leads to an oscillatory motion in many problems [1–3]. Marangoni instabilities have great relevance for many technological areas, including coating techniques [1], liquid microextraction [4], and crystal growth [3,5], among others.

Multicomponent fluids are commonly found in nature and technological applications [6]. The concentration gradients of the components produce not only density gradients but also variations of the surface tension over the interfaces with immiscible fluids. The resulting solutal Marangoni stress (interfacial elasticity) competes with buoyancy to drive the flow around those interfaces, giving rise to intriguing and counterintuitive phenomena, such as the self-propulsion of biological populations [7,8] and active droplets [9,10]. The dynamics of these droplets have been a major focus of earlier studies and illustrate the rich physicochemical hydrodynamics arising in relevant technological fields such as food processing [11].

The flow around an immiscible droplet submerged in a stably stratified mixture of ethanol and water (Fig. 1) is a paradigmatic example of the phenomena described above. In this case, the variation of the interfacial tension over the interface gives rise to a solutal Marangoni stress, which pulls the liquid downward. This effect generates a viscous force acting against gravity that levitates the droplet. The droplet is expected to reach a steady vertical position where the droplet weight is balanced by the buoyancy and viscosity force exerted by the outer fluid. However, when the droplet radius exceeds a certain critical value, the stratification triggers an oscillatory instability of the Marangoni flow, producing the continuous bouncing of the droplet [12–14].

The mechanism responsible for the instability is the following. The Marangoni convection homogenizes the ethanol concentration field around the droplet. The ethanol diffused from the outer bath tries to restore that field (Fig. 1). For droplet radii larger than the critical value, diffusion cannot compensate for the effect of the Marangoni convection, and the concentration field close to the droplet softens. Then, the Marangoni flow weakens and becomes unstable [14].

Li *et al.* [13] conducted the linear stability analysis of the flow described above, assuming Stokes flow and a vanishing capillary number (rigid droplet). The outer viscosity was considered constant, the effect of gravity was modeled with the Boussinesq approximation, and the imposed far-field ethanol concentration was a linear function of the height. Their simulations showed that the system undergoes a Hopf bifurcation at the critical condition. The instability threshold was comparable to that obtained from the experiments.

In this work, we revisit this numerical problem, removing all the above approximations (constant outer viscosity, the Boussinesq approximation, the creeping flow limit, and the rigid droplet approximation). We conduct the linear stability analysis to determine the critical conditions for the oscillatory instability and perform direct numerical simulations to examine the nonlinear time-dependent response of the system. The stability analysis allows us to examine the influence of parameters not considered so far (for instance, the diffusion coefficient). The characteristics of the nonlinear oscillations following the instability are studied from the direct numerical simulations. We explore the parameter space spanned by the droplet radius and viscosity.

II. GOVERNING EQUATIONS

We consider the configuration sketched in Fig. 2. A silicone oil droplet of (constant) density $\rho^{(i)}$, viscosity $\mu^{(i)}$, and volume V is submerged in a large bath containing an ethanol-water mixture. The ethanol-water mixture is linearly stratified under the action of gravity g. Specifically, the ethanol mass

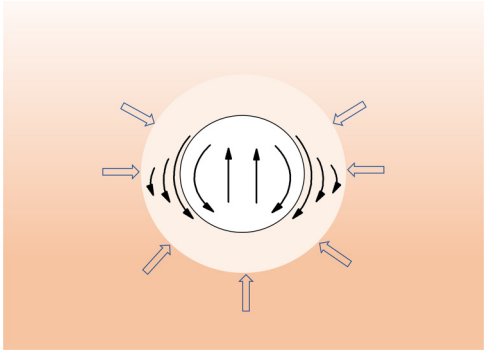

FIG. 1. A sketch of the levitating drop. Deeper orange indicates higher water concentration. The ring around the droplet represents the kinematic boundary layer set by the Marangoni flow indicated by the black arrows. The ethanol concentration inside this layer increases and is homogenized by the Marangoni convection. The blue arrows represent the diffusion of ethanol from the surrounding mixture toward the boundary layer.

fraction Y_e ($0 \leqslant Y_e \leqslant 1$) increases linearly with the vertical coordinate Z. The ethanol-water density $\rho^{(o)}$, viscosity $\mu^{(o)}$, and diffusion coefficient D_e are known functions of Y_e. The interfacial tension γ also depends on the ethanol mass fraction Y_e [15]. The variation of ethanol concentration over the droplet surface produces an inhomogeneous surface tension, which drives the Marangoni flow both inside and outside the droplet.

For a given droplet radius $R_d = [3/(4\pi)V]^{1/3}$, the droplet is expected to reach a stationary vertical position at which the droplet weight is balanced by buoyancy and the viscous force caused by the Marangoni flow. This flow becomes unstable when R_d exceeds a critical value, and the droplet oscillates around the equilibrium position. We solve the steady hydrodynamic equations to find the droplet equilibrium position and conduct the linear stability analysis of the corresponding base flow to determine the critical radius. The time integration of the nonlinear equations allows us to describe the droplet oscillatory behavior following the linear instability.

The hydrodynamic equations are solved in a cylindrical frame of reference (r, z) solidly moving with the droplet's lowest point (see Fig. 2). In this frame of reference, the axisymmetric Navier-Stokes equations are

$$\frac{\partial \rho^{(j)}}{\partial t} + \nabla \cdot (\rho^{(j)} \mathbf{v}^{(j)}) = 0, \tag{1}$$

$$\rho^{(j)} \frac{D\mathbf{v}^{(j)}}{Dt} = -\rho^{(j)} \left(g + \frac{d^2 h}{dt^2} \right) \mathbf{e_z} + \nabla \cdot \boldsymbol{\sigma}^{(j)}, \tag{2}$$

where t is the time, $\mathbf{v}^{(j)} = u^{(j)}\mathbf{e_r} + w^{(j)}\mathbf{e_z}$ is the velocity field, the superscripts $j = i$ and o refer to the inner and outer phases, respectively, and D/Dt is the material derivative. In addition, $h(t) = Z - z$ is the droplet vertical position (see Fig. 2),

$$\boldsymbol{\sigma}^{(j)} = -p^{(j)}\mathbf{I} + \mu^{(j)}[\nabla \mathbf{v}^{(j)} + (\nabla \mathbf{v}^{(j)})^T] \tag{3}$$

is the stress tensor, $p^{(j)}$ is the hydrostatic pressure, and $\mathbf{I}$ is the identity matrix. The ethanol mass fraction Y_e is calculated from the convection-diffusion equation

$$\frac{DY_e}{Dt} = \frac{1}{\rho^{(o)}} \nabla \cdot (\rho^{(o)} D_e \nabla Y_e). \tag{4}$$

The above hydrodynamic equations are solved with the following boundary conditions. The kinematic compatibility condition reads

$$\frac{\partial f}{\partial t} + \mathbf{v}^{(j)} \cdot \nabla f = 0, \tag{5}$$

where $f(\mathbf{r}_i, t) = 0$ determines the interface position $\mathbf{r}_i$. The velocity field must be continuous across the interface, i.e., $\mathbf{v}^{(i)} = \mathbf{v}^{(o)}$. We also impose the balance of normal and tangential stresses at the interface:

$$\mathbf{e_n} \cdot (\boldsymbol{\sigma}^{(o)} - \boldsymbol{\sigma}^{(i)}) \cdot \mathbf{e_n} = \gamma\kappa, \quad \mathbf{e_t} \cdot (\boldsymbol{\sigma}^{(o)} - \boldsymbol{\sigma}^{(i)}) \cdot \mathbf{e_n} = \frac{\partial \gamma}{\partial s}, \tag{6}$$

where $\mathbf{e_n}$ and $\mathbf{e_t}$ are the unit vectors normal and tangential to the interface, respectively, κ is the interface curvature, and s is the meridional arc length. The interfacial tension variation along the droplet surface is calculated as

$$\frac{\partial \gamma}{\partial s} = \frac{d\gamma}{dY_e} \frac{\partial Y_e}{\partial s}. \tag{7}$$

Equation (4) is solved by imposing no diffusive flow of ethanol across the interface, i.e., $\nabla Y_e \cdot \mathbf{e_n} = 0$.

The outer liquid is at rest, and the ethanol concentration $Y_e(Z)$ obeys the prescribed linear relationship $Y_e = 0.229 + 52.58\,Z$ (Z measured in meters) at the outer boundary $r^2 + (z - R_d)^2 = R_o^2$ shown in Fig. 2. Due to the small values of the capillary number (the viscous stress in terms of the capillary pressure), the droplet hardly deforms. In fact, our simulations show negligible deformations with respect to the spherical shape. For this reason, the above expression corresponds to a sphere concentric with the droplet and solidly moves with it (see Fig. 2). The droplet's lowest point is chosen as the origin of the frame of reference, which implies that $u^{(o)} = 0$ and $w^{(o)} = -dh/dt$ at all the points of the outer boundary (see Fig. 2). The regularity conditions $u^{(j)} = \partial w^{(j)}/\partial r =$

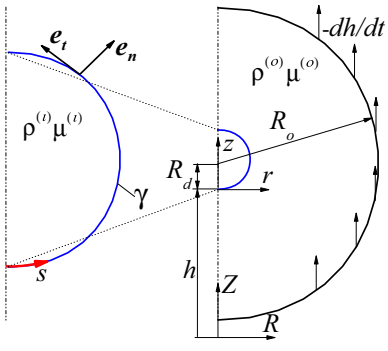

FIG. 2. Sketch of the computational domain. The black semicircumference represents the outer boundary of the numerical domain, which solidly moves with the droplet.

$\partial p^{(j)}/\partial r = \partial Y_e/\partial r = 0$ are considered at the symmetry axis $r = 0$.

The droplet volume must be specified through the following equation:

$$V = \pi \int_0^{s_f} F^2 \left(1 + F_z^2\right)^{-1/2} ds, \tag{8}$$

where s_f is the arc length corresponding to the droplet's upper point, and $F(z)$ is the distance between a surface element and the symmetry axis. Since we chose the droplet's lowest point as the origin of the frame of reference, $w^{(o)} = 0$ at this point. This condition allows us to calculate the droplet's vertical position h_0 in the steady base flow whose linear stability is analyzed.

We considered droplets of silicone oils with different viscosities surrounded by a stratified mixture of ethanol and water. The droplet density is $\rho^{(i)} = 966$ kg/m^3. The constitutive laws $\{\rho^{(o)}(Y_e),\ \mu^{(o)}(Y_e),\ \gamma(Y_e)\}$ are obtained by fitting ninth-degree polynomials to the experimental data reported by Li *et al.* [14], while the data of Seydel *et al.* [16] is used for the diffusion coefficient $D_e(Y_e)$ [15]. The fitting perfectly matches the experimental data for the surface tension. Accurate values of both γ and $d\Gamma/dY_e$ are obtained from this fitting. Therefore, the driving Marangoni stress is calculated accurately. We assume that the interfacial tension $\gamma(Y_e)$ do not significantly depend on the droplet viscosity.

It must be noted that a rigorous dimensional analysis leads to the definition of a large number of dimensionless parameters, including, for instance, the ratio between the characteristic viscosities; the ratio between characteristic densities; the Marangoni, Rayleigh, Reynolds, and capillary numbers (mentioned below); and all the parameters involved in the constitutive laws $\{\rho^{(o)}(Y_e),\ \mu^{(o)}(Y_e),\ \gamma(Y_e)\}$, which depend on the functions used to fit the experimental data. For this reason, we avoid listing all the dimensionless parameters and used dimensional variables to present our results.

The steady solution of the nonlinear equations is calculated using the Newton-Raphson technique. The linear stability of this solution is determined by calculating the axisymmetric eigenmodes. To this end, we assume the temporal dependence

$$\Psi^{(j)} = \Psi_0^{(j)} + \delta\Psi^{(j)}\, e^{-i\omega t} + \text{c.c.}, \tag{9}$$

$$(r_i, z_i) = (r_{i0}, z_{i0}) + (\delta r_i, \delta z_i)\, e^{-i\omega t} + \text{c.c.}, \tag{10}$$

$$h = h_0 + \delta h\, e^{-i\omega t} + \text{c.c.}, \tag{11}$$

where $\Psi^{(j)}(r, z)$ represents the unknowns $\{\mathbf{v}^{(j)}, p^{(j)}, Y_e\}$, and $\Psi_0^{(j)}(r, z)$ and $\delta\Psi^{(j)}(r, z)$ stand for the corresponding base flow (steady) solution and the spatial dependence of the eigenmode, respectively. In addition, (r_i, z_i) denotes the interface position, (r_{i0}, z_{i0}) denotes the interface position in the base flow, and $(\delta r_i, \delta z_i)$ is the perturbation. In the linear stability analysis, one assumes that $|\delta\Psi^{(j)}| \ll |\Psi^{(j)}|$, $|\delta r_i| \ll r_i$, $|\delta z_i| \ll |z_i|$, and $|\delta h| \ll h$. Finally, $\omega = \omega_r + i\omega_i$ is the eigenfrequency characterizing the perturbation evolution. If the growth rate ω_i^* of the dominant mode (i.e., that with the largest ω_i) is positive, then the base flow is asymptotically unstable under small-amplitude perturbations [17]. The flow is stable otherwise. It must be pointed out that since $Z = z + h$, Z at the outer boundary must be perturbed. Therefore, the ethanol concentration $Y_e(Z)$ and the mixture properties $\{\rho^{(o)}(Y_e),\ \mu^{(o)}(Y_e),\ D_e(Y_e),\ \gamma(Y_e)\}$ evaluated at the outer boundary must be perturbed as well.

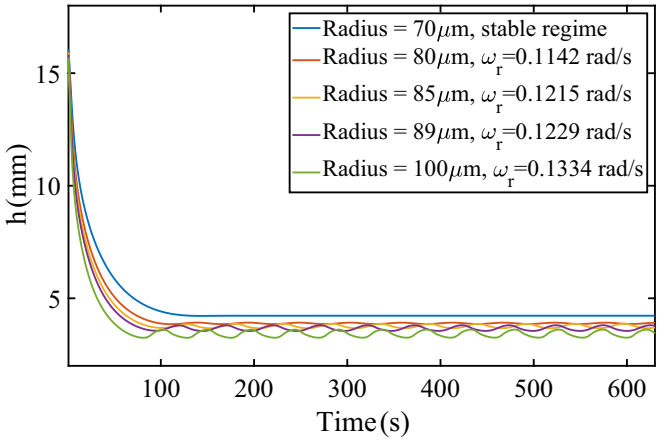

FIG. 3. Droplet vertical position $h(t)$ as a function of time for 100-cSt silicone oil droplets with different radii.

We use the numerical method proposed by Herrada and Montanero [18] to calculate the steady solution and the linear eigenmodes. Details of the mapping and spatial discretization are given in the Appendix. Assuming the temporal dependence of the perturbations in Eqs. (9)–(11), we arrive at the discretized linear system of equations of the generalized eigenvalue problem. The elements of the Jacobian corresponding to that system of equations are symbolic functions calculated by the symbolic package of MATLAB before running the simulation. The eigenvalues are numerically found with the MATLAB function EIGS. In the transient simulations, the temporal derivatives are discretized using second-order backward difference with a constant time step. The resulting system of nonlinear algebraic equations is solved using the Newton-Raphson method. The outer radius of the computational domain is $R_o = 30\, R_d$.

III. RESULTS

We solve the hydrodynamic equations to find the droplet equilibrium position and the steady Marangoni flow sustaining it. Then, we conduct the linear stability analysis of this flow. We also integrate the transient nonlinear equations to study the droplet oscillations around the unstable equilibrium position. We explore the parameter space spanned by the droplet radius R_d and viscosity $\mu^{(i)}$.

Figure 3 illustrates the phenomenon analyzed in this work. It shows the vertical position $h(t)$ of the droplet bottom as a function of time for 100-cSt silicone oil droplets with different radii. In the subcritical case $R_d = 70$ μm, the droplet falls until it levitates steadily, sustained by the Marangoni flow against the apparent droplet weight. In contrast, the supercritical droplets with $R_d \geqslant 80$ μm oscillate periodically due to the instability of the Marangoni flow. The oscillation frequency slightly increases with the droplet radius. We will analyze in more detail the droplet oscillation at the end of this section. Now, we focus on the instability triggering that oscillation.

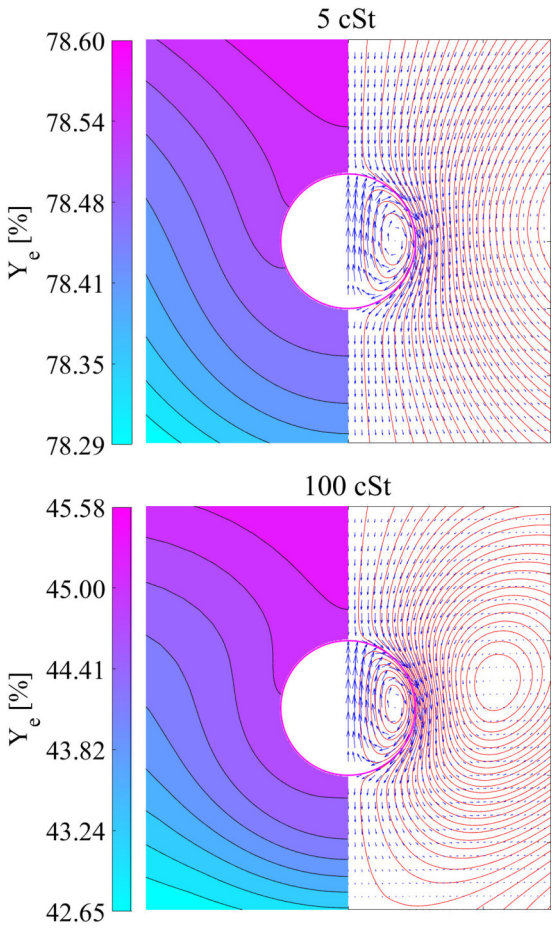

FIG. 4. Ethanol mass fraction Y_e (left) and streamlines (right) for $\{R_d = 39\ \mu\text{m},\ \mu^{(i)} = 5\ \text{cSt}\}$ and $\{R_d = 80\ \mu\text{m},\ \mu^{(i)} = 100\ \text{cSt}\}$. The maximum velocity is 0.423 mm/s and 0.321 mm/s for $\mu^{(i)} = 5$ and 100 cSt, respectively.

Figures 4 shows the approximately marginally stable ($\omega_i^* \simeq 0$) base flows calculated for $\mu^{(i)} = 5$ and 100 cSt. The gradient of surface tension produces Marangoni stresses that drive the liquids on the two sides of the interface from top to bottom. The viscous stress exerted by the outer phase results in an upward force that collaborates with the hydrostatic pressure force to compensate for the droplet weight. The Marangoni flow convects ethanol from the upper to the lower layers reducing the ethanol concentration gradient on the interface. Diffusion tries to restore the imposed far-field concentration gradient. The left-hand sides of the images in Fig. 4 show the result of the competition between ethanol convection and diffusion.

The increase of the droplet viscosity slows down the Marangoni flow. To compensate for this effect, the critical droplet radius increases from 39 μm to 80 μm, and the equilibrium position displaces downward, where the buoyancy force increases. The maximum outer flow velocity takes a larger value for $\mu^{(i)} = 5$ cSt, even though the difference between the ethanol concentrations at the north and south poles is higher for $\mu^{(i)} = 100$ cSt.

Figure 5 shows the spectrum of eigenvalues characterizing the stability of the two base flows described above. The cases

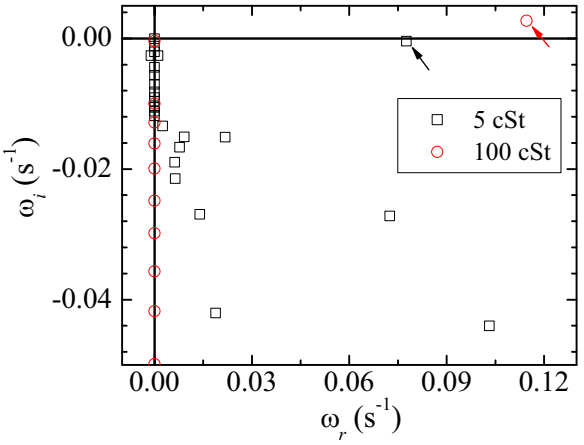

FIG. 5. Spectrum of eigenvalues for $\{R_d = 39\ \mu\text{m},\ \mu^{(i)} = 5\ \text{cSt}\}$ (black squares) and $\{R_d = 80\ \mu\text{m},\ \mu^{(i)} = 100\ \text{cSt}\}$ (red circles). The figure shows the eigenvalues with $\omega_i > -0.05\ \text{s}^{-1}$ and $\omega_r > 0$. The arrows indicate the eigenvalue of the critical eigenmode.

$\mu^{(i)} = 5$ and 100 cSt correspond to a stable flow and an unstable flow. In the former case, $\omega_i < 0$ for all the eigenmodes. In the latter case, one eigenmode has $\omega_i > 0$. This eigenmode is responsible for the instability. The instability is caused by an oscillatory ($\omega_r \neq 0$) critical eigenmode. Therefore, the base flow undergoes a supercritical Hopf bifurcation, leading to the oscillations shown in Fig. 3. As shown below, the frequency of these nonlinear oscillations approximately equals that of the critical eigenmode. The results for the intermediate viscosities are qualitatively the same as those shown in Fig. 5 for $\mu^{(i)} = 5$ and 100 cSt.

There are significant differences between the dominant eigenmodes for $\mu^{(i)} = 5$ and 100 cSt (Fig. 6). The disparity between the inner and outer viscosities in the case $\mu^{(i)} = 100$ cSt increases the magnitude of the outer velocity field perturbation with respect to that in the inner phase. The maximum velocity field perturbation displaces toward the droplet's bottom when the inner viscosity increases. This significantly alters how ethanol transport is perturbed, as observed on the left-hand sides of the images in Fig. 6.

We have explored the parameter space spanned by the droplet radius R_d and viscosity $\mu^{(i)}$. Specifically, we have determined the critical droplet radius as a function of the droplet viscosity. As observed in Fig. 7, the droplet viscosity stabilizes the flow, i.e., the critical radius increases with $\mu^{(i)}$. The critical radii predicted by the linear stability analysis are consistent with the values obtained experimentally [14]. For instance, the theoretical critical radius for a 100-cSt silicone oil is around 77 μm, while the experimental value lies in the interval [60,80] μm [14]. We have also calculated the critical radius for $\mu^{(i)} = 100$ cSt and $dY_e/dZ = 45\ \text{m}^{-1}$. The result is 79 μm, while the experimental value lies in the interval [75, 90] μm. [14].

As mentioned above, diffusion plays a critical role in the Marangoni flow because it tries to restore the imposed far-field concentration gradient to keep the flow running. We have explored the influence of diffusion on the stability conditions by multiplying the diffusion coefficient $D_e(Y_e)$ by a constant

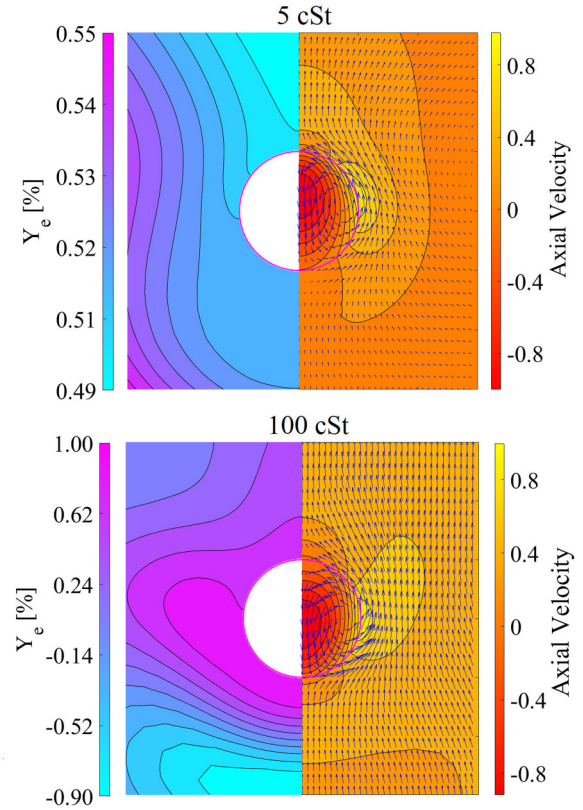

FIG. 6. Real part of the eigenfunction of the ethanol mass fraction Y_e (left) and velocity field (right) for $\{R_d = 39\ \mu\text{m}, \mu^{(i)} = 5\ \text{cSt}\}$ and $\{R_d = 80\ \mu\text{m}, \mu^{(i)} = 100\ \text{cSt}\}$.

factor. Figures 8 and 9 show the critical droplet radius and the maximum velocity of the marginally stable flow as a function of the diffusion coefficient D_e for $Y = 0$. The maximum velocity is reached approximately at the droplet's equator.

For a 5-cSt silicone oil (Fig. 8), the critical radius and the corresponding maximum velocity decrease by the factors 0.42 and 0.24, respectively, when the diffusion coefficient decreases by 0.14. This result is consistent with the instability

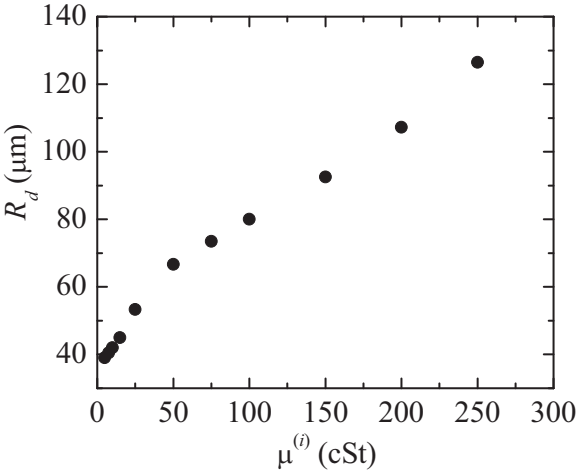

FIG. 7. Critical droplet radius R_d as a function of the droplet viscosity.

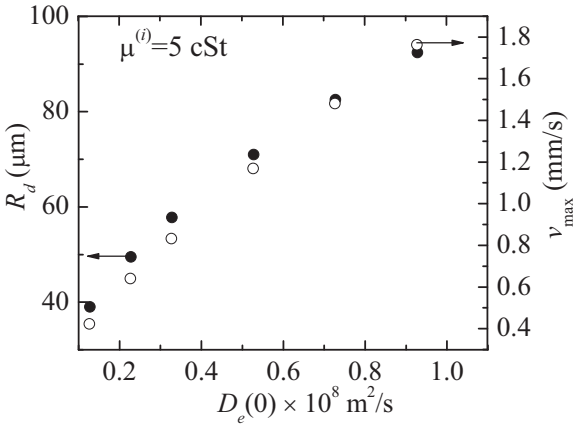

FIG. 8. Critical droplet radius R_d (solid symbols) and maximum velocity $v_{\max}$ (open symbols) as a function of the diffusion coefficient D_e for $Y = 0$. The droplet viscosity is 5 cSt.

mechanism described by Li *et al.* [14]. They claimed that, for small droplet viscosities, the instability is caused by the inability of diffusion to restore the ethanol gradient sustaining the flow around the droplet. Therefore, the reduction of the diffusion coefficient is expected to cause a decrease in the critical radius and $v_{\max}$ of the same order of magnitude.

For a 100-cSt silicone oil (Fig. 9), the critical radius and the corresponding maximum velocity decrease by the factors 0.52 and 0.42, respectively, when the diffusion coefficient decreases by 0.4. This result suggests that the instability is caused by the limited diffusion for $\mu^{(i)} = 100$ cSt as well.

For the case of infinitely large solute diffusivity and zero density gradient, the Marangoni velocity at the equator of the drop is $1/2\,V_M$, where [19]

$$V_M = \left|\frac{d\gamma}{dY_e}\right| \frac{dY_e}{dZ} \frac{R_d}{\mu^{(i)} + \mu^{(o)}}. \tag{12}$$

The quantities $|d\gamma/dY_e|$ and $\mu^{(o)}$ can be evaluated, for instance, at the droplet equator. Using V_M as the characteristic velocity, one defines the Marangoni number $\text{Ma} = V_M R_d / D_e$. The problem is also described in terms of the Rayleigh

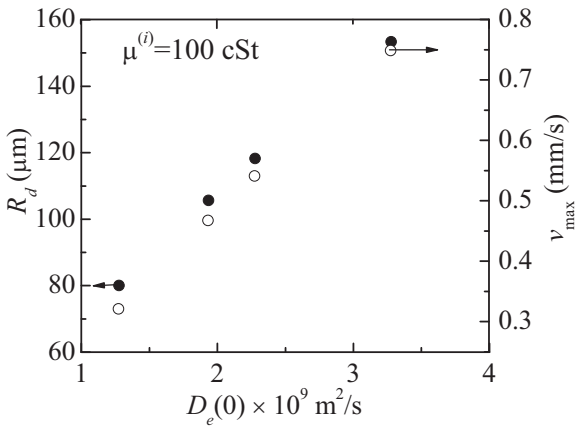

FIG. 9. Critical droplet radius R_d (solid symbols) and maximum velocity $v_{\max}$ (open symbols) as a function of the diffusion coefficient D_e for $Y = 0$. The droplet viscosity is 100 cSt.

number $\mathrm{Ra} = gR_d^4/(\mu^{(o)}D_e)|d\rho^{(o)}/dZ|$. The stability limit can be expressed as

$$f(\mathrm{Ma}, \mathrm{Ra}; \{\mathcal{P}\}) = 0, \tag{13}$$

where $\{\mathcal{P}\}$ represents the rest of dimensionless numbers characterizing the problem.

Li *et al.* [13] explored the parameter space spanned by the concentration gradient dY_e/dZ and the drop radius R_d. They concluded that, for a sufficiently small droplet viscosity, the instability is caused by the limited diffusion of ethanol around the droplet. In this case, the instability criterion is $\mathrm{Ma}/\mathrm{Ra}^{1/2} > c_1$, and c_1 is a constant.

Li *et al.* [14] extended their previous analysis by considering silicone oil droplets of different viscosities (20 cSt, 50 cSt, and 100 cSt). They concluded that, for a sufficiently large droplet viscosity, the flow becomes unstable because the viscous force next to the droplet cannot overcome its buoyancy. This led the authors to the instability criterion $\mathrm{Ra}/\mathrm{Ma} > c_2$, where c_2 is another constant.

Our analysis explored the parameter space spanned by the droplet viscosity $\mu^{(i)}$ and the drop radius R_d. This exploration differs from that conducted by Li *et al.* [14]. Therefore, the dimensionless numbers $\{\mathcal{P}\}$ are varied differently. If these numbers play a significant role, our results cannot reproduce the stability criterion found by Li *et al.* [14].

As shown above, the droplet oscillation (Fig. 3) results from a supercritical Hopf bifurcation suffered by the base flow at the droplet critical radius. The critical eigenmode grows in amplitude until the nonlinear terms in the hydrodynamic equations come into play, fixing the amplitude of the periodic oscillation.

Using V_M defined by Eq. (12) as the characteristic velocity, one defines the Reynolds and capillary numbers

$$\mathrm{Re} = \rho^{(o)}V_M R_d/\mu^{(o)}, \quad \mathrm{Ca} = \mu^{(o)}V_M/\gamma. \tag{14}$$

The quantities $\{|d\gamma/dY_e|, \gamma, \rho^{(o)}, \mu^{(o)}\}$ can be evaluated, for instance, as the values averaged over time at the droplet equator, while dY_e/dZ is the gradient of the unperturbed (far-field) ethanol concentration.

The Reynolds numbers corresponding to the simulations shown in Fig. 3 are smaller than 0.014, implying that the creeping flow approximation holds. In addition, the capillary number takes values below 10^{-4}, meaning the interface hardly deforms. This suggests that the nonlinear term that limits the oscillation amplitude is the convective term of the ethanol diffusive-convective transport equation (4).

In a supercritical Hopf bifurcation, energy is transferred from the base flow to feed the oscillations appearing beyond the critical point. Part of that energy is dissipated by viscosity, reducing the amplitude of the nonlinear oscillations. Figure 10 shows the amplitude of the droplet oscillation as a function of the droplet radius for $\mu^{(i)} = 5$ and 100 cSt. The amplitude of the low-viscosity droplet oscillation is much larger than that of the viscous one. In fact, the amplitude increases quasilinearly with the droplet radius for $\mu^{(i)} = 5$ cSt, reaching values up to two orders of magnitude larger than the droplet radius. Conversely, the amplitude takes an approximately constant value in most of the interval of R_d considered for $\mu^{(i)} = 100$ cSt. This occurs because the viscous dissipation associated with the Marangoni flow inside the droplet considerably reduces the magnitude of the oscillation.

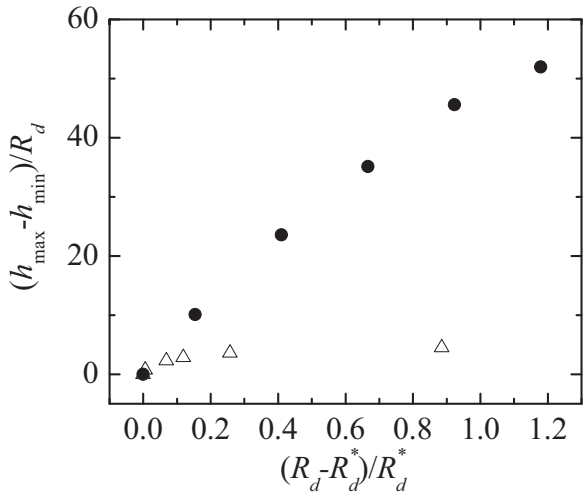

FIG. 10. Amplitude of the droplet oscillation as a function of the droplet radius for $\mu^{(i)} = 5$ (solid symbols) and 100 cSt (open symbols). Here, $h_{\max}$ and $h_{\min}$ are the maximum and minimum values of $h(t)$, respectively, and R_d^* is the critical droplet radius.

The oscillation of the droplet position makes all the relevant quantities oscillate as well. Figures 11 and 12 show the evolution of those quantities evaluated at the droplet's

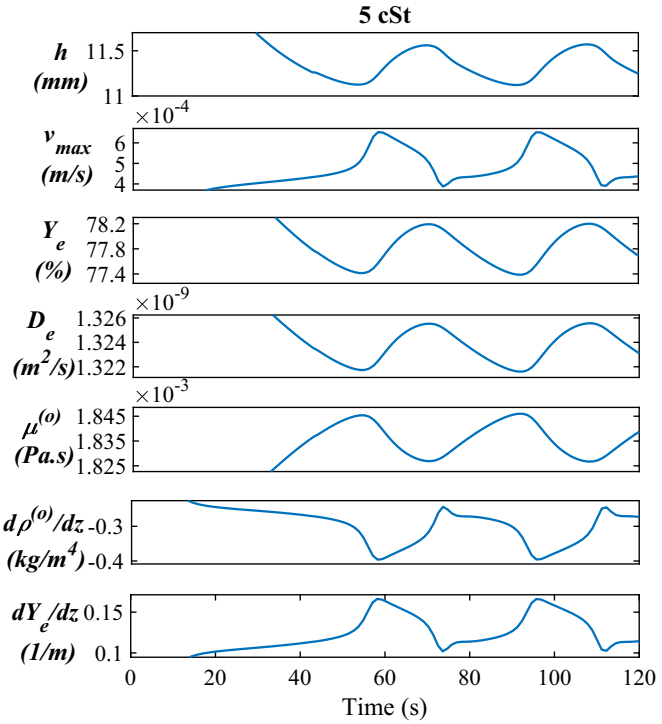

FIG. 11. Droplet vertical position h, velocity at the droplet's equator $v_{\max}$, ethanol concentration Y_e, diffusion coefficient D_e, outer viscosity $\mu^{(o)}$, density gradient $d\rho^{(o)}/dz$, and concentration gradient dY_e/dz as a function of time for $\mu^{(i)} = 5$ cSt and $R_d = 45$ μm. The quantities Y_e, D_e, $\mu^{(o)}$, $d\rho^{(o)}/dz$, and dY_e/dz are evaluated at the droplet's equator.

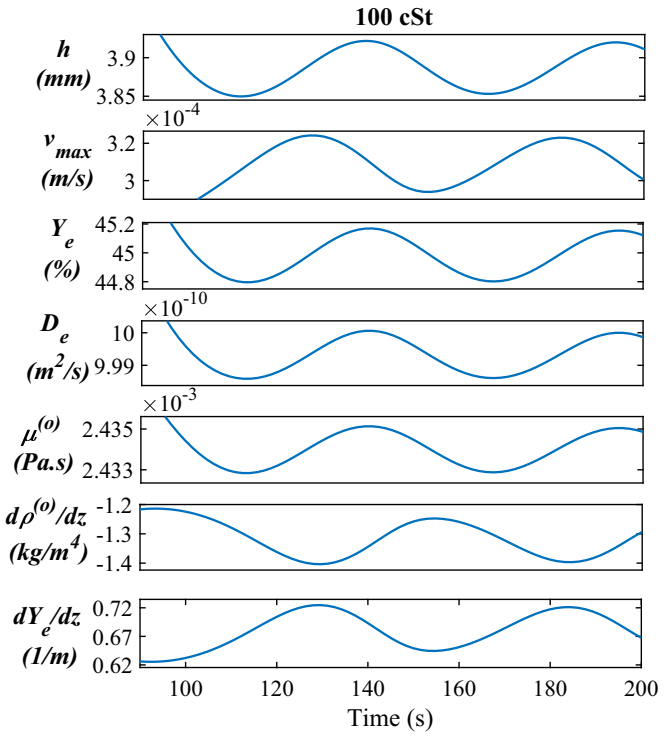

FIG. 12. Droplet vertical position h, velocity at the droplet's equator $v_{\max}$, ethanol concentration Y_e, diffusion coefficient D_e, outer viscosity $\mu^{(o)}$, density gradient $d\rho^{(o)}/dz$, and concentration gradient dY_e/dz as a function of time for $\mu^{(i)} = 100$ cSt and $R_d = 80$ μm. The quantities Y_e, D_e, $\mu^{(o)}$, $d\rho^{(o)}/dz$, and dY_e/dz are evaluated at the droplet's equator.

equator for approximately the critical radii $R_d = 45$ and 80 μm corresponding to $\mu^{(i)} = 5$ and 100 cSt, respectively.

The oscillation for $\mu^{(i)} = 5$ cSt results from the superposition of several harmonics. The frequency of the dominant one shown in Fig. 13, $\omega = 0.1583$ rad/s, is approximately the same as that of the critical eigenmode calculated in the stability analysis, $\omega_r = 0.1552$ rad/s. A quasisinusoidal oscillation is observed for $\mu^{(i)} = 100$ cSt. The frequency of this quasimonochromatic oscillation, $\omega = 0.1105$ rad/s, practically coincides with that of the linear mode responsible for the instability, $\omega_r = 0.1029$ rad/s. The nonmonotonous dependence of D_e and $\mu^{(o)}$ on Y_e [15] explains why the oscillations of D_e and $\mu^{(o)}$ are in antiphase for $\mu^{(i)} = 5$ cSt, while the opposite occurs for $\mu^{(i)} = 100$ cSt.

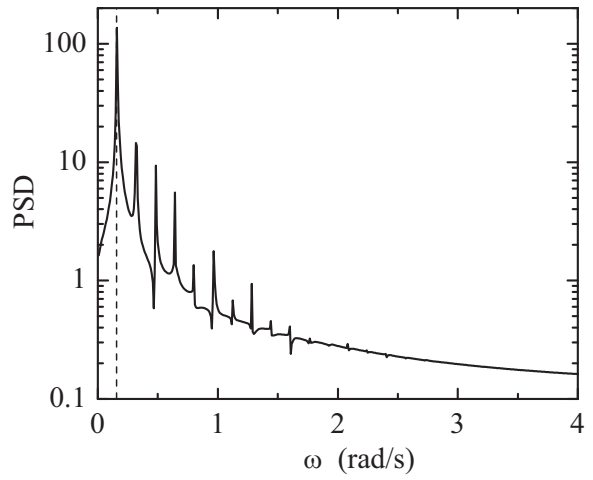

FIG. 13. FFT (Power Spectrum Density, PSD) of the experimental values of $h(t)$ over the time interval [69.76,335.86] s for $\mu^{(i)} = 5$ cSt and $R_d = 45$ μm. The dashed vertical line indicates the frequency of the dominant eigenmode, $\omega = 0.1552$ rad/s.

IV. CONCLUSIONS

We studied numerically the Marangoni flow around an immiscible droplet submerged in a stably stratified mixture of ethanol and water. We conducted the linear stability analysis of the steady base flow to determine the critical conditions for the instability. The base flow undergoes a supercritical Hopf bifurcation that leads to oscillations whose frequency approximately equals that of the critical eigenmode. The numerical predictions for the critical droplet radius were consistent with previous experimental results. We conclude that diffusion is critical in stabilizing the Marangoni flow around both low- and high-viscosity droplets.

The simulations of the nonlinear transient hydrodynamic equations show that the oscillation for the lowest droplet viscosity results from the superposition of several harmonics. However, a quasisinusoidal oscillation is observed in the high-viscosity case. Both inertia and droplet deformation are negligible, which indicates that the convective term of the ethanol diffusive-convective transport equation sets the amplitude of the droplet oscillations. The viscous energy dissipation produced by the Marangoni flow inside the droplet considerably reduces the oscillation amplitude.

The conclusions of the present analysis can be easily generalized to other systems, provided that a vertically stratified liquid generates sufficiently intense Marangoni stress on the droplet surface. The results are expected to be similar to those of thermal Marangoni flows. For instance, the Marangoni convection produced by a temperature gradient and sustaining a bubble submerged in water can suffer from a similar oscillatory instability. Both the linear stability analysis and direct numerical simulations allow one to gain insight into the processes affecting these problems. The possibility of selecting the values of the governing parameters (e.g., the diffusion coefficient) arbitrarily enables one to determine their role in the instability, something almost impossible experimentally.

ACKNOWLEDGMENTS

This research has been supported by the Ministry of Science, Innovation, and Universities under Grants No. PID2019-108278RB and No. PID2022-140951OB.

APPENDIX: MAPPING AND SPATIAL DISCRETIZATION

The inner spatial domain occupied by the droplet is mapped onto a rectangular domain by means of a nonsingular mapping

$$r = f^{(i)}(s, \eta^{(i)}, t), \quad z = g^{(i)}(s, \eta^{(i)}, t), \tag{A1}$$

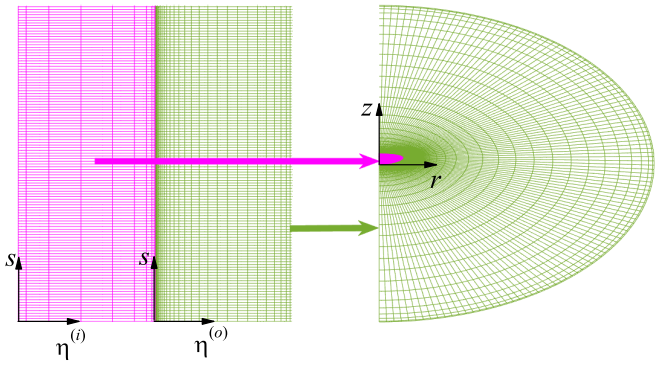

FIG. 14. Computational subdomains and grids for the original and mapped variables. The green (magenta) lines represent the oil (water-ethanol) mesh in the real space (right panel) and in the computational domain (left panel).

where $[0 \leqslant s \leqslant 1]$ and $[0 \leqslant \eta^{(i)}, \leqslant 1]$ are the normalized arc length and mapped radial coordinates, respectively. The shape functions $f^{(i)}$ and $g^{(i)}$ are obtained as a part of the solution by using a quasielliptic transformation [20]. Some additional boundary conditions for these shape functions are needed to close the problem [21].

The interface is located at $\eta^{(i)} = 1$. Therefore, its parametric representation, $r_s = F(s,t)$ and $z_s = G(s,t)$, verifies the equations

$$f^{(i)}(s,1,t) = F(s,t), \quad g^{(i)}(s,1,t) = G(s,t). \tag{A2}$$

Here, r_s and z_s are the cylindrical coordinates of an interface point in the real space. The functions F and G are obtained by imposing the kinematic compatibility condition (5)

$$\left(u^{(i)} - \frac{\partial F}{\partial t}\right)\frac{\partial G}{\partial s} - \left(w^{(i)} - \frac{\partial G}{\partial t}\right)\frac{\partial F}{\partial s} = 0, \tag{A3}$$

and the equation

$$\frac{\partial F}{\partial s}\frac{\partial^2 F}{\partial s^2} + \frac{\partial G}{\partial s}\frac{\partial^2 G}{\partial s^2} = 0, \tag{A4}$$

which guarantees a uniform distribution of the points along the arc length s.

At the axis $\eta^{(i)} = 0$, the following equations are satisfied

$$f^{(i)}(s,0,t) = 0, \quad \frac{\partial^2 g^{(i)}}{\partial^2 s}(s,0,t) = 0. \tag{A5}$$

The outer spatial domain occupied by the ethanol-water mixture is also analytically mapped onto a rectangular domain in the form

$$r = F(s,t) + (R_o - F(s,t))\eta^{(o)}, \quad z = G(s,t), \tag{A6}$$

where $[0 \leqslant \eta^{(o}, \leqslant 1]$ is the mapped radial coordinate.

All the derivatives appearing in the governing equations are expressed in terms of t and the spatial coordinates (s, η) resulting from the mapping. These equations are discretized in the η-direction with $n_\eta^{(i)} = 11$ and $n_\eta^{(o)} = 61$ Chebyshev spectral collocation points [22] in the inner and outer regions, respectively. We use fourth-order finite differences with $n_s = 121$ equally spaced points to discretize the s direction (Fig. 14).

[1] J. R. A. Pearson, "On convection cells induced by surface tension," J. Fluid Mech. **4**, 489 (1958).

[2] A. Y. Rednikov, P. Colinet, M. G. Velarde, and J. C. Legros, "Two-layer benard-marangoni instability and the limit transverse and longitudinal waves," Phys. Rev. E **57**, 2872 (1998).

[3] H. C. Kuhlmann, *Thermocapillary Convection in Models of Crystal Growth* (Springer-Verlag, Berlin, 1999)

[4] A. Jain and K. K. Verma, "Recent advances in applications of single-drop microextraction: A review," Anal. Chim. Act **706**, 37 (2011).

[5] D. Schwabe and A. Scharmann, "Some evidence for the existence and magnitude of a critical Marangoni number for the onset of oscillatory flow in crystal growth melts," J. Cryst. Growth **46**, 125 (1979).

[6] P. Li and J. Zhang, "Finite-difference and integral schemes for maxwell viscous stress calculation in immersed boundary simulations of viscoelastic membranes," Biomech. Model. Mechanobiol. **19**, 2667 (2020).

[7] L. E. Scriven and C. V. Sternling, "The Marangoni effects," Nature (London) **187**, 186 (1960).

[8] F. Yang, S. Shin, and H. A. Stone, "Diffusiophoresis of a charged drop," J. Fluid Mech. **852**, 37 (2018).

[9] A. Y. Rednikov, Y. S. Ryazantsev, and M. G. Velarde, "Active drops and drop motions due to nonequilibrium phenomena," J. Non-Equilib. Thermodyn. **19**, 95 (1994).

[10] C. C. Maass, C. Kruger, S. Herminghaus, and C. Bahr, "Swimming droplets," Annu. Rev. Condens. Matter Phys. **7**, 171 (2016).

[11] B. M. Degner, K.M. Olson, D. Rose, V. Schlegel, R. Hutkins, and D. J. McClements, "Influence of freezing rate variation on the microstructure and physicochemical properties of food emulsions," J. Food Eng. **119**, 244 (2013).

[12] Y. Li, C. Diddens, A. Prosperetti, K. L. Chong, X. Zhang, and D. Lohse, "Bouncing oil droplet in a stratified liquid and its sudden death," Phys. Rev. Lett. **122**, 154502 (2019).

[13] Y. Li, C. Diddens, A. Prosperetti, and D. Lohse, "Marangoni instability of a drop in a stably stratified liquid," Phys. Rev. Lett. **126**, 124502 (2021).

[14] Y. Li, J. G. Meijer, and D. Lohse, "Marangoni instabilities of drops of different viscosities in stratified liquids," J. Fluid Mech. **932**, A11 (2022).

[15] See Supplemental Material at http://link.aps.org/supplemental/10.1103/PhysRevE.108.065104 for the dependence of the mixture properties on the ethanol concentration.

[16] T. Seydel, R. M. Edkins, and K. Edkins, "Picosecond self-diffusion in ethanol–water mixtures," Phys. Chem. Chem. Phys. **21**, 9547 (2019).

[17] V. Theofilis, "Global linear instability," Annu. Rev. Fluid Mech. **43**, 319 (2011).

[18] M. A Herrada and J. M. Montanero, "A numerical method to study the dynamics of capillary fluid systems," J. Comput. Phys. **306**, 137 (2016).

[19] N. O. Young, J. S. Goldstein, and M. J. Block, "The motion of bubbles in a vertical temperature gradient," J. Fluid Mech. **6**, 350 (1959).

[20] Y. Dimakopoulos and J. Tsamopoulos, "A quasielliptic transformation for moving boundary problems with large anisotropic deformations," J. Comput. Phys. **192**, 494 (2003).

[21] M. A. Herrada, Y. E. Yu, and H. A. Stone, "Global stability analysis of bubbles rising in a vertical capillary with an external flow," J. Fluid Mech. **958**, A45 (2023).

[22] M. R. Khorrami, M. R. Malik, and R. L. Ash, "Application of spectral collocation techniques to the stability of swirling flows," J. Comput. Phys. **81**, 206 (1989).